Sensor mapping of Amazonian Dark Earths in deforested croplands

Mats Söderström [a,f,*], Jan Eriksson [b], Christian Isendahl [c], Denise Pahl Schaan [d], Per Stenborg [c], Lilian Rebellato [e], Kristin Piikki [a,f]

[a] Department of Soil and Environment, Swedish University of Agricultural Sciences, Box 234, SE-532 23 Skara, Sweden
[b] Department of Soil and Environment, Swedish University of Agricultural Sciences, Box 7014, SE-750 07 Uppsala, Sweden
[c] Department of Historical Studies, University of Gothenburg, Box 200, SE-405 30 Gothenburg, Sweden
[d] Universidade Federal do Pará, Rua Augusto Correa 1, CEP 66075-110 Belem, PA, Brazil
[e] Department of Anthropology and Archaeology, Universidade Federal do Oeste do Pará, Rua Vera Paz s/n, Salé 68040-250 Santarém, PA, Brazil
[f] International Center for Tropical Agriculture (CIAT), Kasarani Rd., , ICIPE Complex, PO Box 823-00621, Nairobi, Kenya

ABSTRACT

Amazonian Dark Earths (ADEs) are fertile soils for agricultural production as well as important archaeological resources for understanding the pre-Columbian past of the Neotropical lowland rainforest. ADEs are threatened by expanding land exploitation and there is a need to develop efficient approaches to soil mapping and analysis for documenting these soils. In this paper we assess the potential of satellite remote sensing and proximal soil sensing to map, predict and monitor ADEs in land affected by agro-industrial development. We use instruments based on portable x-ray fluorescence (PXRF) and electromagnetic induction (EMI) as well as high-resolution satellite data (Spot 6) for detailed soil surveys at a 10-ha ADE site now mainly used for soybean production on the Belterra Plateau, Pará, Brazil. We predict the regional occurrence of ADE in a c. 250 km² test area centred on the known ADE site São Francisco using satellite data. Multivariate adaptive regression splines models were parameterised for predictions of soil organic carbon (SOC), cation exchange capacity (CEC), phosphorus (P) and depth of the A horizon in ADEs from sensor data – both from individual sensors and in sensor combinations. Combining sensors gave the best validation results: the highest modelling efficiencies (E) were 0.70 (SOC), 0.88 (CEC) and 0.74 (for both P and A depth). The most powerful single proximal sensor outputs in the predictions were Sr from the PXRF data and magnetic susceptibility (MSa) as measured by the EMI instrument. In the regional satellite based model we located 17 previously unrecorded ADE sites >2 ha. Ground control checks showed that 10 out of 11 sites were correctly classified. We conclude that these sensors are useful in studies of ADE in deforested cropland and provide new opportunities for detailed studies of the archaeological record.

1. Introduction

Amazonian Dark Earths (ADEs; also known as *terras pretas*) rich in nutrients, organic matter and carbon in the very stable form of biochar (pyrogenic carbon) are unique agricultural resources distinct from the strongly weathered soils that dominate in the Amazon. ADEs are of great interest as providers of important ecosystem services and as multi-facetted and rich archaeological sources of information that have helped to revise the interpretation of pre-Columbian Amazonia. ADEs contain high frequencies and densities of cultural artefacts, and archaeological and pedological investigations demonstrate that ADEs

have formed as a result of human activities mainly during the later pre-Columbian period (c. CE 0–1500) (Glaser and Birk, 2012; Steiner et al., 2004; Woods and Denevan, 2010). Owing to their capacity to sequester carbon and hold soil nutrients ADEs form important models for current efforts to produce soils with similar qualities, particularly in the tropics (Lehmann, 2007; Lehmann and Joseph, 2009; Verheijen et al., 2010). In Amazonia, ADE patches vary in size from under a hectare to several hundred hectares and are highly valued by farmers, both smallholders and large-scale soybean producers. Incited by regional and national economic growth interests and the demand for protein fodder in the global livestock industry, ADEs have increasingly been brought under agro-industrial cultivation (Morton et al., 2006; Richards et al., 2015). The expansion of agro-industrial production has propelled intense debates over environmental and social impacts and load displacements (e.g. Hornborg, 2009). As part of this critique it has largely been assumed rather than shown in detail that agro-industrial land management erodes the long-term conservation of both the agricultural and archaeological properties of ADEs. In the Santarém-Belterra

* Corresponding author at: Department of Soil and Environment, Swedish University of Agricultural Sciences, Box 234, SE-532 23 Skara, Sweden.
E-mail addresses: mats.soderstrom@slu.se (M. Söderström), jan.o.eriksson@slu.se (J. Eriksson), christian.isendahl@gu.se (C. Isendahl), schaandenise@gmail.com (D.P. Schaan), per.stenborg@gu.se (P. Stenborg), lilian.rebellato@ufopa.edu.br (L. Rebellato), kristin.piikki@slu.se (K. Piikki).

region of the Brazilian Amazon in western Pará, deforestation associated with cash-crop mono-cropping for national and global fodder markets and cattle breeding for meat production has precipitated fundamental landscape change over the last decades (Fig. 1) (Corrêa et al., 2011); the inauguration of a modern grain terminal for oceanic transportation at the port of Santarém in 2003 facilitated this development. Based on current understanding of the distribution of ADE sites in this region (Nimuendajú, 2004; Söderström et al., 2013; Stenborg et al., 2012) we know that land clearance often will, intentionally or unintentionally, make ADEs available to agro-industrial farming. In the face of the on-going exploitation of land in the region it is of fundamental concern to develop methods for mapping, predicting and assessing how large-scale cultivation using modern methods affect the archaeological and pedological record, as well as to monitor its effects on soil quality.

Despite an increasing volume of inter-disciplinary ADE research over the last two decades regional and local-scale mapping of ADE is fragmentary and remains largely in its infancy. Current distribution maps indicate clustering on floodplain bluffs of major rivers and near current population centres, such as at the soybean frontier in the Santarém-Belterra area (McMichael et al., 2014), but there may be a bias towards accessible areas (WinklerPrins and Aldrich, 2010). Hence, there is a need to develop efficient approaches to soil mapping and analysis for

documenting ADEs. In recent years, digital soil mapping (DSM) has been developed as a cost-efficient approach to predict spatial patterns of soil properties across geographical scales by integrating quantitative methods with proximal and remote sensing imagery, soil data and other covariates such as digital elevation data (Boettinger, 2010; Minasny et al., 2008). DSM is particularly useful in regions, such as the Amazon, where the available information on the quality of land and soil resources that guides land-use planning is often fragmentary and coarse in resolution; in the Amazon region only very general soil maps are available except in smaller areas where more detailed surveys have been carried out (Fearnside and Leal Filho, 2001; Quesada et al., 2011; Teixeira et al., 2008).

Thayn et al. (2011) discuss the possibility to use satellite based remote sensing for locating ADE in forested parts of the Amazon Basin, in particular by correlating differences in vegetation composition with soil quality, thus distinguishing forest on ADE soils from forest on the relatively poor soils that dominate the region. Another far more straightforward approach is to use satellite-based remote sensing in areas with limited vegetation, such as those cleared for mechanized agriculture. Mostly applied in local-scale studies, proximal soil sensing (PSS; when sensors are used in close contact with or within a distance of a few meters from the soil) is a way to rapidly and often non-
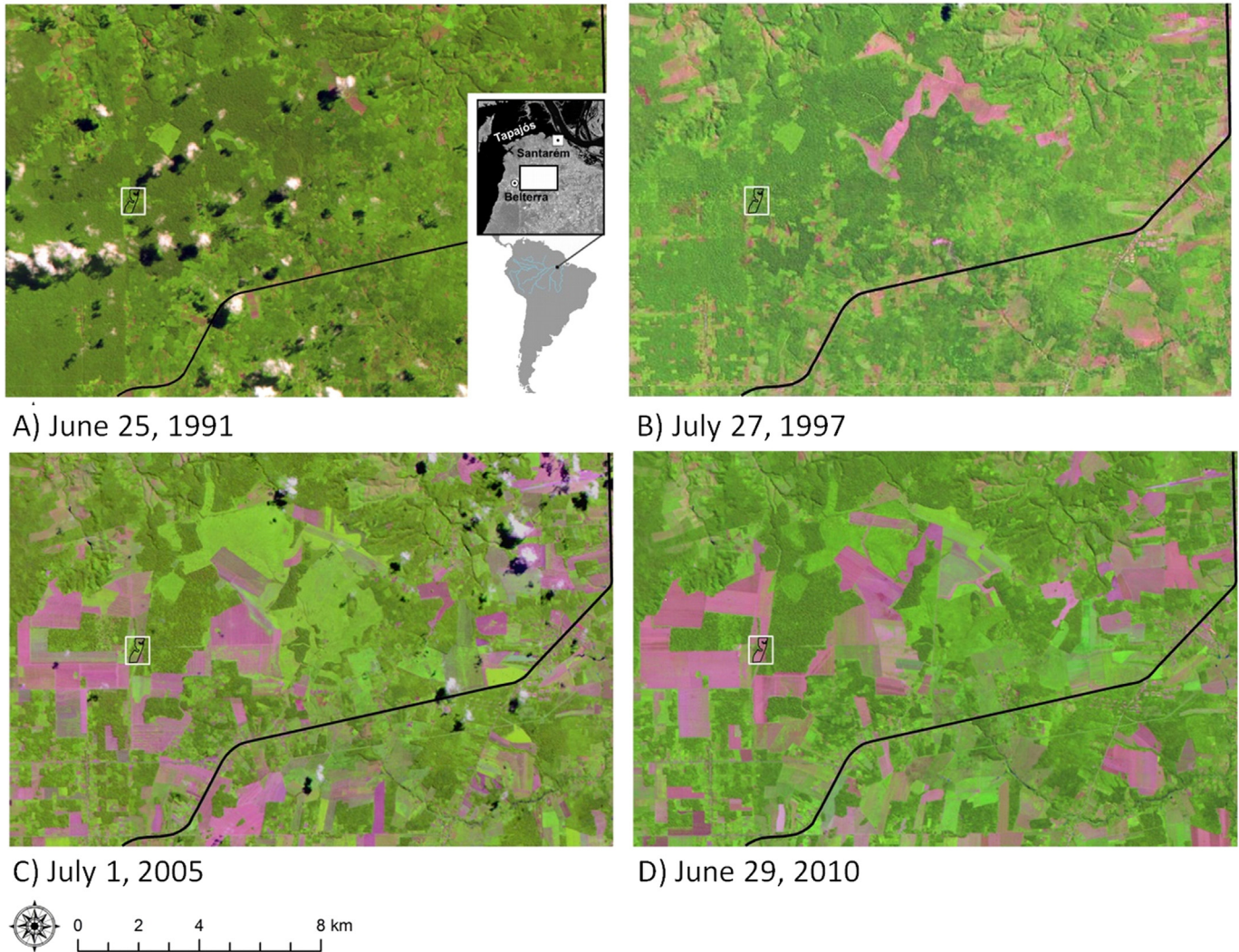

A) June 25, 1991
B) July 27, 1997
C) July 1, 2005
D) June 29, 2010

0   2   4   8 km

Fig. 1. A–D. Land-use change in the Amazon near the confluence of the Tapajós and Amazon Rivers (see inset in A). Over this 19 year period the character of land use changes from small-scale, forest-fallow smallholder agriculture and forest to large fields of mechanized agriculture dominated by soybean production. Landsat 5 images 1991–2010 of the Belterra Plateau study area south of Santarém city in Pará, Brazil. Colour and structure can be used for interpretation, e.g.: dark green = forest; large, homogenous light green areas = agricultural land with vegetation; violet = agricultural fields without vegetation. The black line represents road BR-163. The white square shows the location of Fig. 2. (For interpretation of the references to colour in this figure legend, the reader is referred to the web version of this article.)

destructively measure different soil properties directly or indirectly on the soil surface or of a given soil volume. PSS instruments can for example be based on reflectance of visible and near infrared radiation, x-ray fluorescence, gamma radiation or electrical conductivity (Adamchuk et al., 2015).

The objective of this study was to assess the potential to use different soil sensing techniques–satellite remote sensing and proximal soil sensors, separately and in combination–for mapping exploited ADEs. This forms an important step towards a better understanding of how mechanized agriculture impacts the long-term maintenance of soil properties and the archaeological record of pre-Columbian Amazonian social-ecological systems. The ultimate goal of this study is to provide an operational case study for how such sensing methods can be employed both regionally and locally for rapid appraisal of the occurrence of ADEs in areas that have been subjected to deforestation and subsequent conversion to agricultural land.

2. Materials and methods

2.1. Study area

The study comprises a 256 km^2 area on the Belterra Plateau, some 30 km south of the city of Santarém in the state of Pará, Brazil (Fig. 1). The Belterra Plateau is an upland environment elevated about 150 m above the Amazon and Tapajós river floodplains that geologically is part of the Cretaceous Alter do Chão Formation (Irion, 1984). ADE occurs in patches surrounded by Ferralsols that dominate the region in general. The study area consists both of secondary forest and large, open fields dominated by modern, mechanized soybean and maize production. In the secondary forest local smallholders practice shifting cultivation that results in a mosaic of vegetation with mostly shrub and medium-high forest. Most of the large fields were opened up in this area during a rapid expansion of soybean production in the first decade of this century (Fig. 1).

A total of six ADE sites at least partly located in fields cleared for large-scale agricultural production were known from an earlier archaeological survey in the study area (Stenborg et al., 2012). A detailed soil survey was conducted in November and December 2012 at São Francisco, an ADE site to the most part situated within an agricultural field under mechanized production of soybeans and maize. Archaeological data suggest that São Francisco formed a small settlement with at least three probable house complexes located adjacent to a circular depression probably of pseudokarstic origin, c. 40 m in diameter and about 2 m deep, possibly modified and used as reservoir. Similar features are common in the Belterra region (Stenborg et al., 2014). Results from the preliminary analysis of the excavated material suggest a date of occupation to c. CE 1000–1500.

2.2. Data for regional prediction mapping of ADE occurrence

A model for predicting ADE occurrences in areas of non-vegetated arable land (further described in Section 2.6 Statistical analyses) under mechanized production was made based on data from a high-resolution satellite image (Spot 6, Airbus Defence and Space, Toulouse, France) from November 27, 2012 (at the time of field work) with spectral bands: panchromatic (PAN; 450–745 nm), blue (B; 450–525 nm), green (G; 530–590 nm), red (R; 625–695 nm) and near-infrared (NIR; 760–890 nm). Spot 6 images have a spatial resolution of 1.5 m in the panchromatic band and 6 m multispectrally. To reduce the impact of varying radiance levels between fields due to differences in management, the radiance of each spectral band of the satellite data were field-wise level-adjusted (the average radiance of a field was set to the average of the surrounding fields). The three visible bands were highly correlated and recalculated to a visible light similarity index (SI_{SAT}) estimated as the inverse of the standard deviation of the digital numbers of B, G and R (Eq. 1). This index, which will become higher if

one of the bands differ from the others, was used together with data from the PAN and the NIR band in the regional modelling instead of the individual visible bands.

$$SI_{SAT} = Stdev(B, G, R)^{-1} \qquad (1)$$

2.3. Detailed soil survey

Detailed soil surveys (including soil sampling, soil profile descriptions and measurements with two different types of sensors) were carried out in November and December 2012 at São Francisco, where the ADE soil extends over slightly >10 ha, most of which is within an open arable field under soybean and maize cropping using modern agricultural methods. Transects for soil sampling were manually laid out guided by visual assessments of ADE properties (dark colour and presence of pottery sherds on the surface; Fig. 2). The transects were placed to cover both ADE and Ferralsol areas and were oriented NW-SE so that they would not coincide with the windrows from tillage of the field and strings of ashes from recent burning of vegetation residues (remnants from when the field was cleared from vegetation about 10 years ago; visible as stretches of dark soil colour in Fig. 2). Reference soils without any visible anthropic influence other than present-day farming (samples no. 55–59 in Fig. 2) were sampled some distance away from the area covered by the transects. Soil samples (0–20 cm depth) were taken with an auger at sample points located every 40 m along the transects. In total 65 soil samples were collected, eight in the forested area and the rest in the agricultural field. Where the A-horizon was thicker than 20 cm, 20–40 cm depth was also sampled (30 locations). At each sampling location a composite sample consisting of three cores was taken in a triangle with a side of approximately 2 m, and the depth and the Munsell colour of the A-horizon were noted. A number of soil profiles were also sampled, described and classified according to the World Reference Base for Soil Resources (IUSS Working Group WRB, 2014). One set of soil profile pits were dug to study a sequence from more brownish to more blackish anthropic soil (samples no. 101–104 in Fig. 2). In these soil profiles description and sampling (in the profile wall) was made down to 50 cm depth. Profile description and sampling was also made of one of the reference soils (sample no. 105 in Fig. 2) following the same protocol. Three soil profiles were also described and sampled (e1, e3, and e4 in Fig. 2) in archaeological test-pit excavations. In all soil profiles sampling depths were determined by the genetic horizons. All soil samples were air-dried at 45 °C and sieved through a 2 mm mesh previous to laboratory analyses. The positions of pits and sampling points were registered by a TDS Nomad GPS (Tripod Data Systems, Corvallis, OR, USA).

2.4. Soil laboratory analyses

Soil pH was measured both in water and KCl in a soil:solution ratio of 1:2.5; the soil organic carbon (SOC) content was determined by wet oxidation with K-dichromate with a modified Walkley & Black method (Embrapa, 2009); extractable P by Mehlich 1 (0.05 M HCl + 0.05 H$_2$SO$_4$); exchangeable calcium (Ca^{2+}), potassium (K$^+$) and magnesium (Mg^{2+}) were extracted with 1 M calcium acetate at pH 7; and exchangeable aluminium (Al^{3+}) with 1 M KCl. The exchangeable cations were analysed with atomic absorption spectrophotometry (AAS). Exchangeable acidity (H$^+$ + Al^{3+}) was determined volumetrically by a back-titration of the acetate extract with NaOH, using phenolphthalein as indicator. Contents of sand (2–0.05 mm), silt (0.05–0.002 mm) and clay (<0.002 mm) were determined by wet sieving and densiometer-sedimentation measurements, using calcium hexametaphosphate 0.1 M and sodium hydroxide 0.1 M as dispersing agents (Gee and Bauder, 1986). Cation exchange capacity (CEC) at pH 7 and base saturation (BS) were calculated from analyses of base cations and exchangeable acidity.
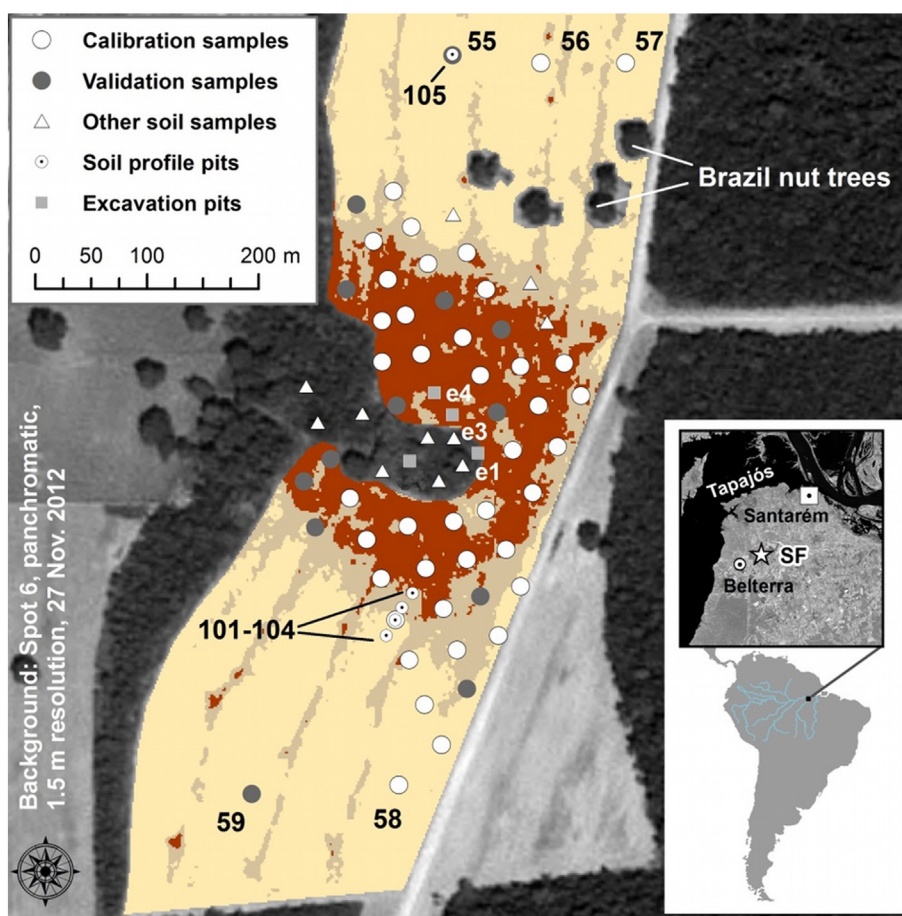
Fig. 2. The São Francisco (SF) ADE site north-east of Belterra. The field background is a panchromatic satellite image (Spot 6, November 27, 2012) classified in three classes according to greyscale level in the image. Limits were assigned to the 20th and the 40th percentile of the grey scale levels which subjectively fitted well with the visual impression during field work (which was the basis for placement of transects and sampling sites): dark red-brown background = strongest ADE character; light brown background = weaker ADE character; light yellow = reference soil without ADE character. Labelled samples are mentioned in the text. (For interpretation of the references to colour in this figure legend, the reader is referred to the web version of this article.)

2.5. Proximal soil sensors

Two types of non-invasive geophysical instruments were used for soil scanning in the field:

I. A sensor based on electromagnetic induction (EM38-MK2; Geonics Ltd., Mississauga, ON, Canada) that registers the apparent soil electrical conductivity (ECa in mS m^{-1}) at two depths simultaneously, mainly 0–0.5 m and 0–1 m depth, denoted ECa05 and ECa10 respectively, as well as values proportional to the apparent magnetic susceptibility (MSa), denoted MSa05 and MSa10. MSa has an effective depth about half of that of ECa (the depth response of MSa with this type of instrument have been discussed e.g. in Clark, 1990; Benech and Marmet, 1999; Simpson et al., 2010) (Fig. 3A).

II. A portable x-ray fluorescence (PXRF) analyser (Niton XL3t GOLDD+; Themo Scientific, Billerica, MA, USA) for detection of the total concentrations of many elements in samples of about half a cubic cm of soil (Fig. 3B).

EM38 measurements were made at a duration of 15 s at 60 of the soil sampling points (53 in the agricultural field and seven in the forested area) with the instrument 15 cm above the ground ($z = 15$) and also placed directly on the ground surface ($z = 0$). Since response functions are non-linear the response depth of the sensors will change if the instrument height changes. Consequently, this method of measurement resulted in four values of ECa and MSa at each soil sampling point. The position of the EM38 was registered by a TDS Nomad GPS (Tripod Data Systems, Corvallis, OR, USA).

PXRF measurements were made on the soil surface at the same soil sampling locations as the EM38 measurements, using the Test-all-geo calibration (specific for the Thermo Scientific instrument) which is suitable for quick scanning of a broad range of elements in soils, returning concentrations and measurement standard deviations on 45 elements starting from Mg and heavier. The limit of detection (LOD) is suggested as three times the returned standard deviation (Weindorf et al., 2012a). PXRF measurements in soil are affected by a number of conditions such as water content and structure (Potts and West, 2008), suggesting that measurements directly in the field may be relatively uncertain in absolute terms. However, in this case obtaining absolute concentrations was not the ultimate goal, merely to include PXRF data as auxiliary data for predictions of some key ADE properties. Three measurements were done at each soil sample location (at the locations where the subsample soil core was subsequently obtained), and the average of the element concentrations was used. Measurement time was four minutes in total for each PXRF measurement (one minute per filter), i.e. twelve minutes per sampling site. Seven of the elements from the PXRF measurements (Al, Ca, Fe, Si, Nb, Sr and Th) were used in further analyses and modelling. These were all above the LOD (on average 3.8 [Ca] to 20 [Fe and Nb] times > the measurement standard deviation) and also correlated ($p < 0.05$) to at least one of the ADE properties modelled in this research.

2.6. Statistical analyses

Maps as well as spatial and image analyses were carried out in ArcGIS 10 (ESRI Inc., Redlands, CA, USA) with the extension Spatial Analyst. Linear regression was used for testing the use of single sensor

Fig. 3. Proximal soil sensors used: A) EM38-MK2 (Geonics Ltd., Mississauga, ON, Canada) for measuring soil electrical conductivity and magnetic susceptibility (photo: Christian Isendahl); B) Niton XL3t GOLDD+ (Themo Scientific, Billerica, MA, USA), a portable x-ray fluorescence (PXRF) analyser for detection of the total concentrations of many elements (photo: Mats Söderström).

outputs for predictions of key ADE soil properties (CEC, SOC, thickness of the A horizon and P; lnP was used since the data distribution was very skewed). A data mining method, multivariate adaptive regression splines (MARSplines; Hastie et al., 2009), was used for combining sensor outputs in multivariate prediction models. The package Earth (Milborrow, 2015) in the R software (R Core Team, 2014) was used for MARSplines modelling, a form of non-parametric regression in which the data are divided into a number of piece-wise linear splines (H_m) that are split at break points (t):

$$H_m = (x-t)_+ = \begin{cases} x-t & x>t \\ 0 & otherwise \end{cases} \tag{2}$$

The ADE properties studied (Y_{ADE}) were estimated as a function of the predictors (x). The intercept parameter β_0 was added to the weighted (by βm) sum of M basis functions and their interactions (k):

$$y_{ADE} = f(x) = \beta_0 + \sum_{m=1}^{M} \beta_m H_{km}(x_{(k,m)}) \tag{3}$$

To make as simple models as possible no interactions were allowed ($k = 1$). To reduce the risk of over-fitting, a built-in pruning function was used to remove functions that did not substantially contribute to the prediction accuracy.

The soil data from the arable field at São Francisco was randomly divided into a calibration dataset (n = 40) and a validation set (n = 13; Fig. 2). In addition to testing univariate prediction models, based on each of the sensor outputs (the linear regression analysis), four different sets of predictors from the sensors were used individually or in combination (Table 1) in MARSplines models for each ADE property.

All models were validated by making predictions for the validation samples, and the statistics mean absolute error (MAE), root mean square error of prediction (RMSEP) and the Nash-Sutcliffe model efficiency (E; indicates how well a plot of observed and predicted values fit the 1:1-line; Nash and Sutcliffe, 1970) were calculated.

In the regional modelling only the presence or absence of ADE on land under mechanized agricultural production without vegetation at the time of image acquisition was predicted, also through MARSplines modelling. For the predictions a regional dataset was used consisting of about 1.3 million grid points with the spectral information from the multispectral Spot 6 satellite image corresponding to the centre of the 6×6-m^2 cells (the data used for the regional modelling is described in Section 2.2 and in Table 1). For calibration and validation, a binary dataset was produced consisting of 120 of the grid points, of which 60 were randomly chosen within the six known ADE locations (from the study of Stenborg et al. (2012); the extent of these sites was verified by visual inspection) and assigned 1, and the other half (assigned 0) arbitrarily located outside these ADE sites. Hence, at each known ADE site there were 10 points assigned 1 and ten points assigned 0. All 20 points belonging to an ADE site were removed at a time for calibration and subsequent validation. A calibration model based on all calibration sites were then applied onto the entire regional prediction dataset, which yielded a map of likelihood (0–1) of ADE at any grid point in the region. For ground truth validation eleven of the predicted ADE locations were visited in October 2014. It was assessed whether the soil was an ADE or not on the basis of visual, qualitative inspection of the occurrence of pre-Columbian ceramic sherds, the presence of charcoal and soil colour on the surface. The selection of sites for field assessment was based on accessibility.

3. Results

3.1. Detailed soil survey at the São Francisco ADE site

3.1.1. Soil properties and soil classification

There were clear gradients in topsoil properties along the soil sampling transects, from the reference soils towards the soils with increasingly pronounced ADE character (Table 2). Average SOC content was 42 mg kg^{-1} in the most developed ADEs on arable land in the São Francisco area, compared to 23 mg kg^{-1} in non-anthropic soils. CEC was also highest in the most developed ADEs. The pH-H$_2$O also increased, from 5.3 in reference soils to 6.6 in the ADEs, and thus acidity decreased and BS increased accordingly. Higher CEC and higher BS in the ADE also mean that concentrations of exchangeable cations were considerably higher than in the reference soil samples (for correlation coefficients see Table 3). Phosphorus concentrations were much higher in the ADEs than in the reference soils. Soil analyses of the samples from the forest area indicated that most of them had a pronounced ADE character. Disregarding the five reference soils, over 80% of the sampled soils had a P concentration of 30 mg kg^{-1} or higher, which is required for classification as a pretic surface horizon according to IUSS Working Group WRB (2014). A pretic horizon must also have a depth of 20 cm or more. The medium developed ADEs, according to the colour classification in Fig. 2, had an average A-horizon depth of 22 cm in the auger cores. Half of the locations had an A-horizon depth ≥ 20 cm. Three quarters of the strongly developed ADEs had an A-horizon ≥20 cm; in two sites it was 40 cm and the average depth was 25 cm. The deepest A-horizon (54 cm) was recorded in excavation pit 3 (e3 in Fig. 2).

Table 1
Predictor sets used in MARSplines modelling, both individually and in combination, at São Francisco. Z refers to the distance in cm above the ground at which the instrument was positioned while measuring.

Predictor set	Sensor	Predictors
a	PXRF	Al$_{PXRF}$; Ca$_{PXRF}$; Fe$_{PXRF}$; Si$_{PXRF}$; Nb$_{PXRF}$; Sr$_{PXRF}$; Th$_{PXRF}$
b	EMI (Z = 15)	ECa10$_{z15}$; ECa05$_{z15}$; MSa10$_{z15}$; MSa05$_{z15}$
c	EMI (Z = 0)	ECa10$_{z0}$; ECa05$_{z0}$; MSa10$_{z0}$; MSa05$_{z0}$
d	Satellite	PAN$_{SAT}$; SI$_{SAT}$; NIR$_{SAT}$

Table 2
Summary statistics of soil properties at São Francisco. Averages and standard deviations (within parentheses) for the 0–20 cm layer unless otherwise specified. The classification into weak, medium and strong ADE is shown in Fig. 2. SOC = soil organic carbon, BS = degree of base saturation.

	n	A-depth cm	SOC g kg^{-1}	pH-H$_2$O	pH-KCl	P mg kg^{-1}	lnP
All soils	65	23 (8)	37 (10)	6.3 (0.5)	5.5 (0.4)	117 (119)	4.3 (1.0)
Arable soils	57						
Reference	5		23 (3)	5.3 (0.3)	4.6 (0.3)	23 (5)	3.1 (0.3)
ADE weak	9	20 (8)	27 (3)	6.2 (0.5)	5.4 (0.5)	36 (23)	3.4 (0.6)
ADE medium	17	22 (6)	37 (10)	6.4 (0.3)	5.6 (0.3)	88 (106)	4.1 (0.8)
ADE strong	26	25 (7)	42 (8)	6.6 (0.3)	5.7 (0.3)	180 (124)	5.0 (0.7)
Forest soils	8	24 (11)	40 (14)	6.0 (0.3)	5.3 (0.3)	122 (131)	4.2 (1.2)
ADEs with an A-horizon thicker than 20 cm							
0–20 cm layer	28	–	45 (9)	6.4 (0.4)	5.7 (0.3)	170 (133)	4.8 (1.0)
20–40 cm layer	28	–	24 (5)	6.2 (0.4)	5.4 (0.3)	113 (111)	4.2 (1.0)

	Al^{3+}	Ca^{2+}	K$^+$	Mg^{2+}	Acidity	CEC	BS
	mmol$_c$ kg^{-1}						%
All soils	<1	99 (38)	3.5 (1.6)	19 (7)	33 (15)	155 (37)	76 (15)
Arable soils							
Reference	3 (2)	38 (7)	1.7 (0.4)	7 (2)	56 (9)	102 (12)	45 (6)
ADE weak	<1	61 (32)	3.4 (1.6)	13 (4)	35 (18)	113 (23)	66 (18)
ADE medium	<1	97 (30)	4.0 (1.4)	20 (6)	30 (12)	151 (29)	79 (11)
ADE strong	<1	125 (22)	4.0 (1.3)	23 (3)	27 (9)	179 (22)	85 (6)
Forest soils	<1	100 (30)	2.5 (2.0)	22 (11)	44 (21)	168 (41)	74 (10)
ADEs with an A-horizon thicker than 20 cm							
0–20 cm	<1	127 (23)	4.3 (1.7)	24 (5)	29 (16)	184 (23)	84 (8)
20–40 cm	<1	75 (23)	2.1 (1.1)	15 (5)	30 (13)	122 (26)	75 (10)

A non-anthropic reference soil (no. 105 in Fig. 2) in the NW part of the study area was classified as Xantic Ferralsol (Clayic, Hyperdystric, Vetic) (IUSS Working Group WRB, 2014; data and soil profile descriptions of soils mentioned in this section are presented in Eriksson et al. (2016)). This is the same classification as non-anthropic soils in proximity to another ADE location (at Bom Futuro) 15 km SW of the São Francisco study site (Söderström et al., 2013), except for an Acric prefix qualifier at Bom Futuro which could not be determined in the São Francisco soil. Our general impression is that this part of the Belterra Plateau is dominated by this type of very clayey Ferralsols. The proposed classification of the soils in the excavation pits is Pretic Anthrosol (Clayic, Eutric, Ferralic). For the soil in the deepest excavation pit (e3 in Fig. 2) Eutric can be detailed to Hypereutric, while the other two soils presumably are Epieutric and Orthoeutric respectively (depths below 77 and 59 cm respectively were not sampled). The sequence of

Table 3
Soil properties correlation coefficient (r) matrix* of all soil samples shown in Fig. 2 (n = 65). For units, see Table 2.

	SOC	pH–H$_2$O	pH–KCl	lnP	Ca^{2+}	K$^+$	Mg^{2+}	Acidity	CEC
pH–H$_2$O	0.39								
pH–KCl	0.47	0.79							
lnP	0.60	0.52	0.60						
Ca^{2+}	0.78	0.63	0.78	0.80					
K$^+$	0.49	0.51	0.50	0.50	0.55				
Mg^{2+}	0.78	0.55	0.59	0.56	0.82	0.53			
Acidity	−0.21	−0.72	−0.76	−0.51	−0.63	−0.35	−0.48		
CEC	0.87	0.47	0.61	0.73	0.94	0.56	0.86	−0.34	
BS	0.56	0.76	0.88	0.68	0.88	0.50	0.75	−0.87	0.71

* Probability values: Dark grey box = p < 0.001, light grey box = p < 0.01;
white box = p <0.05; grey italic = p ≥ 0.05

*Probability values: Dark grey box = p < 0.001, light grey box = p < 0.01; white box = p < 0.05; grey italic = p ≥ 0.05.

soil profile pits along the gradient of increasing ADE character in the southern part of the area (no. 101–104 Fig. 2) had A-horizon depths of around 20 cm. A depth of 20 cm in combination with fulfilment of other criteria, e.g. a colour value ≤4 and a chroma ≤3 and a Mehlich P content of >30 mg kg^{-1}, show that these have a diagnostic Pretic horizon, but it is not thick enough for classification as Anthrosol. In an Anthrosol the antropogenic horizon should be at least 50 cm thick. The classification would be Pretic Xantic Ferralsol (Clayic, Hyperdystric, Vetic).

3.1.2. Sensors for mapping ADE properties at São Francisco

It was more efficient to combine sensors in comparison to using single sensor outputs for predictions of SOC, CEC, lnP and depth of the A horizon (A depth). Validation statistics for the best predictor sets and the best single predictors for each sensor are shown in Table 4. Concerning the single sensors, strontium determined by the PXRF (Sr$_{PXRF}$) was the single most useful element measured by that sensor; in particular lnP and CEC could be predicted relatively well with a simple linear model of Sr$_{PXRF}$. In the combined predictor set models, also Fe$_{PXRF}$, Ca$_{PXRF}$ and Al$_{PXRF}$ were included in different models but not Nb$_{PXRF}$ and Th$_{PXRF}$. When calibrating a MARSplines model, not all predictors in a set are forced into the model, only useful predictors are included. For the EMI instrument, it was MSa10$_{z0}$ that was most often included in prediction models. Also the readings of MSa10$_{z15}$ and ECa10$_{z15}$ were often included, i.e. values from the coil configuration rendering the deepest measurements and when the instrument was held 15 cm above the ground. The shallow measurements were seldom included in the multivariate prediction models. However, the best validation statistics for A depth (MAE 4.3 cm; RMSEP 5.3 cm; E 0.70) was achieved with a model that combined MSa05$_{z0}$ and MSa10$_{z0}$ (Eq. (4)).

$$\begin{aligned} A\ depth_c = {} & 24.21 - 0.32 \times \max(0; MSa05_{z0} - 48.47) - 0.62 \\ & \times \max(0; 48.47 - MSa05_{z0}) + 1.09 \\ & \times \max(0; MSa10_{z0} - 20.80) \end{aligned} \quad (4)$$

The best sensor combination to predict CEC according to the validation statistics were PXRF (Ca$_{PXRF}$, Sr$_{PXRF}$ and Fe$_{PXRF}$) and the EMI

Table 4

Validation statistics for the best performing combinations of sensors (predictor sets; predictors in Table 1) and the best single predictor for CEC (mmol$_c$ kg^{-1}), SOC (mg kg^{-1}), lnP (mg kg^{-1}) and depth of the A horizon (A depth; cm). The predictor sets refer to data from different sensors: a = PXRF; b = EMI (Z = 15 cm); c = EMI (Z = 0 cm); d = satellite (details in Table 1).

	Predictor	MAE	RMSEP	E
CEC				
	Combined predictor sets[1]			
	ab	9.5	12.9	0.88
	abcd	11.6	14.5	0.84
	cd	12.9	15.5	0.82
	Best single predictor[2]			
	Sr$_{PXRF}$	14.6	20.6	0.68
	MSa10$_{z15}$	17.9	20.8	0.68
	MSa10$_{z0}$	18.0	20.5	0.69
	NIR$_{SAT}$	22.4	25.1	0.53
lnP				
	Combined predictor sets[1]			
	acd	0.35	0.51	0.74
	abd	0.37	0.51	0.74
	b	0.41	0.53	0.71
	Best single predictor[2]			
	Sr$_{PXRF}$	0.46	0.52	0.73
	ECa10$_{z15}$	0.51	0.62	0.62
	ECa10$_{z0}$	0.53	0.61	0.62
	NIR$_{SAT}$	0.56	0.69	0.52
	Predictor	MAE	RMSEP	E
SOC				
	Combined predictor sets[1]			
	bd	4.3	5.3	0.70
	a	4.4	6.0	0.63
	ab	4.8	6.0	0.62
	Best single predictor[2]			
	Sr$_{PXRF}$	5.4	6.7	0.53
	MSa10$_{z15}$	6.5	7.6	0.39
	MSa10$_{z0}$	6.5	7.6	0.39
	PAN$_{SAT}$	5.0	6.0	0.62
A depth				
	Combined predictor sets[1]			
	d	4.4	5.0	0.74
	c	4.4	5.1	0.74
	a	4.4	5.2	0.72
	Best single predictor[2]			
	Sr$_{PXRF}$	6.0	7.4	0.44
	MSa10$_{z15}$	5.5	6.4	0.58
	MSa10$_{z0}$	5.9	6.8	0.53
	NIR$_{SAT}$	5.2	6.2	0.61

[1] Combined predictor sets were used in MARSplines models
[2] Single predictors were used in linear regression models.

instrument held at 15 cm above the ground (MSa10$_{z15}$) (combined predictor set ab; letters explained in Table 1) which resulted in the values MAE = 9.5 mmol$_c$ kg^{-1}, RMSEP = 12.9 mmol$_c$ kg^{-1} and E = 0.88 (Eq. (5)).

$$CEC_{ab} = 145.79 + 5.49 \times 10^{-3} \times \max\left(0; Ca_{PXRF} - 5.06 \times 10^4\right) + 6.12 \times 10^{-3} \times \max\left(0; 3.74 \times 10^4 - Fe_{PXRF}\right) - 3.26 \times \max(0; 28.29 - Sr_{PXRF}) + 2.52 \times \max(0; MSa10_{z15} - 20.76) \quad (5)$$

Reflectance from the ground surface as registered by the Spot 6 satellite was also often well correlated to the analysed ADE indicators, but was less commonly selected by the data mining method in the combined models. However, the single best predictor for SOC and A depth were the satellite PAN and NIR predictors, respectively. In the best performing combined models for SOC, the satellite PAN predictor combined with sensor reading from the EMI instrument held at 15 cm

height (ECa05$_{z15}$ and MSa05$_{z15}$) were included (combined predictor set bd: MAE 4.3 g kg^{-1}; RMSEP 5.3 g kg^{-1}; E 0.70) (Eq. (6)).

$$SOC_{bd} = 32.51 + 1.85 \times \max(0; ECa05_{z15} - 11.00) + 1.06 \times \max(0; MSa10_{z15} - 18.50) - 0.07 \times \max\left(0; PAN_{SAT} - 8.43 \times 10^2\right) \quad (6)$$

For lnP it was a combination of registrations from all sensors (Ca$_{PXRF}$, ECa10$_{z0}$ and NIR$_{SAT}$) that gave the best results (combined predictor set acd: MAE 0.35 mg kg^{-1}; RMSEP 0.51 mg kg^{-1}; E 0.74) (Eq. (7)).

$$lnP_{acd} = 4.084 + 2.40 \times 10^{-4} \times \max\left(0; Ca_{PXRF} - 5.06 \times 10^3\right) - 0.30 \times \max(0; 12.79 - ECa10_{z0}) - 1.63 \times 10^{-2} \times \max\left(0; 1.003 \times 10^3 - NIR_{SAT}\right) \quad (7)$$

Scatterplots of observed and predicted values of CEC, SOC, lnP and A horizon depth of the best models are shown in Fig. 4A-D.

3.2. Regional mapping of ADE in agricultural land

A significant part of the 250 km^2 area covered by the satellite images used at São Francisco was open agricultural land. In the Spot 6 image acquired at the time of field work, slightly >5100 ha of such land had very little vegetation (light green fields in Fig. 6), and that area was possible to use for the modelling of ADE distributions. The best calibration model for the regional probability prediction of Amazonian Dark Earths (ADE$_p$) included the predictors based on the panchromatic satellite band and the visible-light similarity index (Eq. (8)):

$$ADE_p = 0.968 + 1.13 \times 10^{-3} \times \max(0; 870 - PAN_{SAT}) + 4.31 \times 10^{-1} \times \max\left(0; SI_{SAT} - 5.33 \times 10^{-2}\right) - 9.61 \times 10^{-3} \times \max(0; PAN_{FLA} + 117) + 9.29 \times 10^{-3} \times \max(0; PAN_{FLA} + 20) \quad (8)$$

where PAN$_{FLA}$ is the field-wise level-adjusted radiance of the panchromatic band. Results of the cross-validation process are displayed in Fig. 5, which shows that for predicted probabilities above 0.4, all validated sites were ADE. The map produced by the final calibration model based on all calibration data presented in Fig. 6 shows reclassified ADE predictions (ADE criteria used: predicted likelihood >0.6 and ADE area > 2500 m^2). The areal threshold removed most of the strips of recently burnt material (as those shown in light brown in Fig. 2), which otherwise were frequently classified as ADE. In total 99 sites (except for the calibration ADE sites) larger than 2500 m^2 were classified as ADE, with a total coverage of 170 ha. Seventeen of these sites were larger than 2 ha.

Eleven of the mapped ADE sites were visited in the field in October 2014 (site nos. 1–11 in Fig. 6). All but one (number 10 in Fig. 6) could with certainty be assessed as an ADE according to soil colour, presence of pottery sherds and occurrence of charcoal on the soil surface. The largest predicted site in the study area covered 20.5 ha (site number 11 in Fig. 6). However, judged from the shape and general appearance in the map, some of the predicted sites are likely to be strips of recently burnt material from the clearing of the land (e.g. south of the São Francisco site in Fig. 6). Nevertheless, these sites represent only a small part of the classified sites.

4. Discussion

Our results from this and previous studies (Araújo et al., 2015; Söderström et al., 2013) show that it is possible to make rapid but still quite detailed mapping of ADE sites using different kind of sensors. EMI instruments are increasingly used in detailed soil surveys in the framework of precision agriculture. Most frequently it is the soil
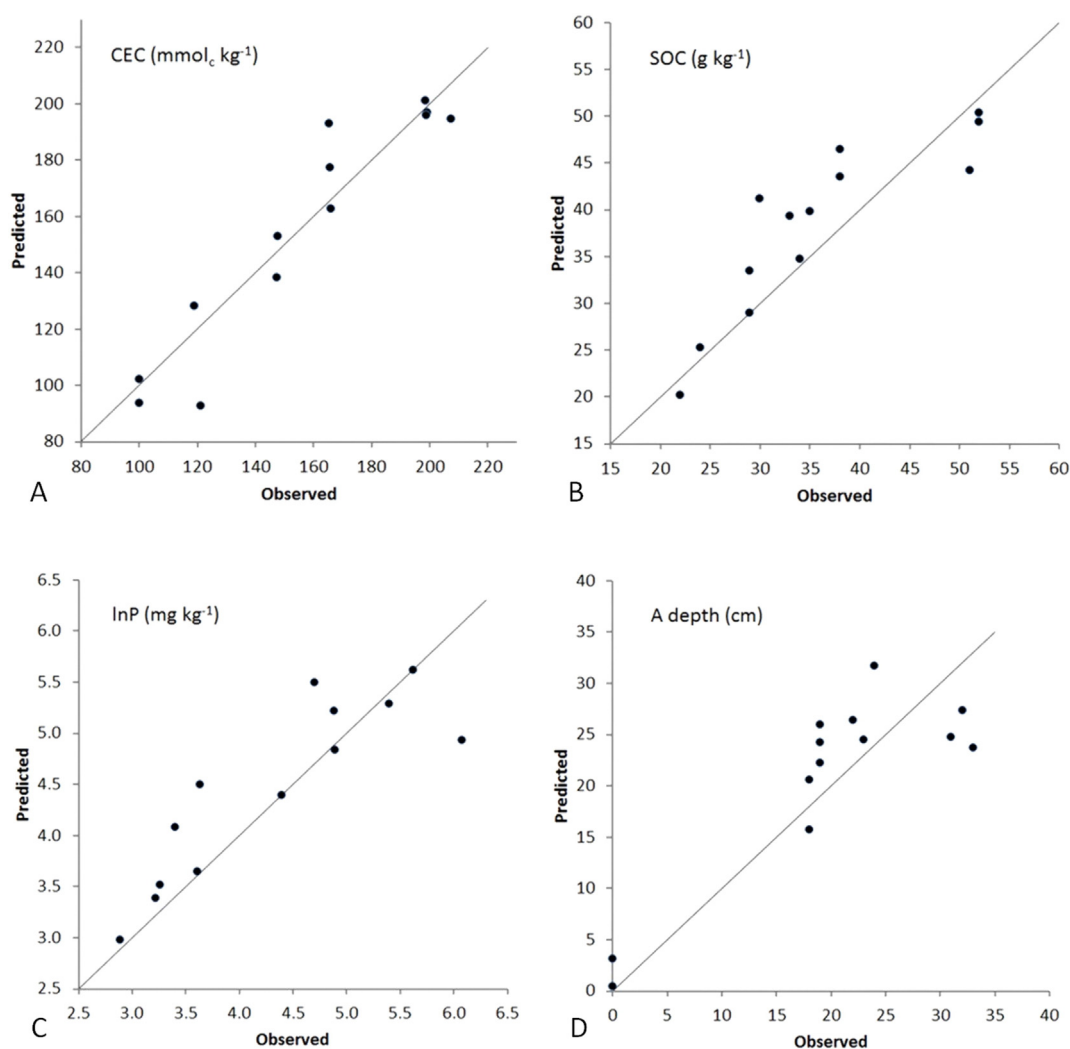
Fig. 4. Validation plots of the best prediction models for CEC, SOC, lnP and depth of the A horizon.

apparent electrical conductivity (ECa) that is used. In the soils of the study area, however, the apparent magnetic susceptibility (MSa) is particularly useful to discriminate ADE from the background soil. Frequent burning of soil producing soil temperatures >400 °C may in the presence of soil organic matter transform iron oxides to magnetic minerals, such as magnetite and maghemite, and a number of studies indicate that prolonged prehistoric occupation can result in elevated levels of magnetic susceptibility of affected soils (Blake et al., 2006; Jordanova et al., 2001; Söderström et al., 2013; Tite and Mullins, 1971; Marwick, 2005). High MSa is a useful marker of burning residues associated with settlement and land use activities of the indigenous Amazonian population during the time of ADE formation. In forested areas, where it is more difficult to visually inspect the ground compared to agricultural fields, a non-invasive instrument that measures MSa is efficient for rapidly mapping the extent of ADE sites (Söderström et al., 2013). The deeper measurements of the EMI sensor (ECa10 and MSa10) were more often included in the prediction models used in this study, than were the more shallow registrations (ECa05 and MSa05). Holding the instrument 15 cm above the ground or putting the instrument on the ground did not produce major differences in the correlations, although the ground predictors ($z = 0$) were more often selected in the prediction models when sensors were combined. Especially in densely vegetated terrain it is difficult to hold the instrument at a constant height if measurements are done continuously while walking. Since the effective measurement depth is affected by the height of the instrument, it may

in such cases be advantageous to place the instrument on the ground to reduce registration noise.

Data from both the ground sensors and the satellite image were correlated to a number of key ADE properties. However, since many of these key properties were also strongly correlated with each other, these results should be interpreted with some caution. A key property of ADEs is the accumulation of pyrogenic C, contributing to SOC. Both the satellite images and the EMI measurements are affected by the content of SOC. Since the soils in the studied area appeared to be rather homogenous with a strongly weathered mineralogy (also indicated by Irion, 1984), it can be assumed that there is little variation in the CEC of the mineral soil. Thus the spatial variation of the CEC of the soil should mainly be determined by SOC. In the ADE soil analyses there is thus a strong correlation between CEC and SOC (Table 3). Therefore, there is also a strong correlation between satellite data and EMI data and CEC. The PXRF does not measure SOC or CEC, but our data indicate that it can be used to predict CEC and indirectly SOC, as also shown in Weindorf et al. (2012b). In that study, Sr was consistently included in regression analyses between SOC and PXRF data at three different locations in North America.

In our case, measurements of Sr was the best single predictor for CEC (Table 4). Ca and Sr are geochemically strongly associated (Bowen and Dymond, 1955) (in this case $r^2 = 0.70$ between Ca_{PXRF} and Sr_{PXRF}), and the PXRF measurements of Sr and Ca were more or less equally well related to the key ADE indicators examined. A presumable reason
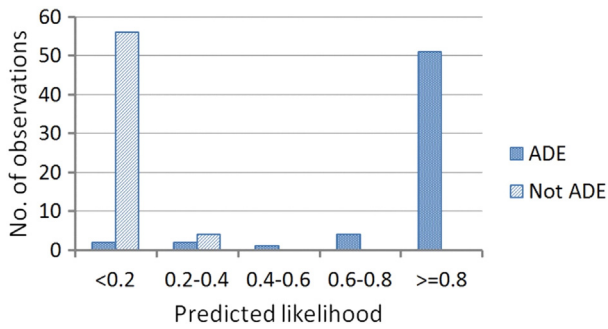
Fig. 5. Results of cross-validation of the regional prediction model of ADE on arable land. One ADE site out of six was removed at a time, and the calibration model for the remaining sites was deployed to estimate the likelihood for the 20 observation points (10 ADE and 10 non-ADE) at the withheld site.

why Sr performed slightly better in the prediction models is that these values were more stable than the Ca values; the Sr concentrations measured by the PXRF were on average 6 times higher than the returned standard deviation, compared with <4 times higher for Ca. A possible reason for the observed relationship to CEC is that the amount of Ca^{2+} and Sr^{2+} (the latter ion at a much lower concentration level though) adsorbed on the exchange complex is higher the higher the CEC. In our data there is a very strong correlation between exchangeable Ca^{2+} and CEC (Table 3). However, the PXRF measurements should reflect the total Ca and Sr concentration in the soil. The presumable reason why total Ca and Sr in this case reflects the CEC of the soil is that a major part of these elements present in the soil is retained in exchangeable form to the negatively charged soil particles. The background Ferralsol at the SF site contain only small amounts of Ca-minerals (about 2000 mg kg^{-1} according to the PXRF measurements), which is typical for the strongly weathered upland soils in the Amazon Basin (Curi and Franzmeier, 1987; Irion, 1984; Sombroek, 2000).

Al$_{PXRF}$ and Fe$_{PXRF}$ were negatively correlated to the soil properties that are typical indicators of ADE. Fe was, together with Ca and MSa, included in the best prediction model for CEC. Even if the PXRF instrument only measures a soil surface area of about 1 cm^2 and has a measurement depth of a few millimetres, the values obtained indicated the general conditions in the topsoil; mixing of the soil through cultivation practices is likely beneficial in this case.

In this paper we have showed that satellite images are a powerful tool to detect ADEs in arable land with bare soil, and thereby it is possible to better understand their distribution regionally. This is not surprising since these soils have very different reflectance characteristics compared to the yellowish or reddish Ferralsols that dominate in the region (shown in Table 4). Assuming that 90% of the mapped ADE sites are correctly classified in the regional study (which is a reasonable estimation based on the results of the cross-validation (Fig. 5) and the field assessment of the predictions), and that the investigated area is representative for the Belterra Plateau, ADE covers about 3% of the total land area in this region. This figure corresponds to a recent estimate by McMichael et al. (2014). They presented a probability model of ADE occurrences over the entire Amazon basin and concluded that about 3% had the conditions that made ADE formation possible. In our current understanding of ADE distributions throughout the Amazon region, most sites, as well as the largest sites recorded, are located on lower, non-flooded floodplain bluffs (WinklerPrins and Aldrich, 2010). This study, as well as those of, e.g., Mann (2002); Stenborg et al. (2012), and Schaan (2016), indicate that earlier assessments of the distribution of ADE sites focusing on locations in near proximity to the main waterways of the central Amazon may be fragmentary and at least partly a result of survey bias. In this study area, as many as 17 "new" ADE sites larger than 2 ha were identified by modelling of remote sensing data, clearly demonstrating the utility of remote sensing approaches to understand Amazon soil and pre-Columbian settlement distributions.

A major lacuna in our current understanding of the management and stewardship of ADE soils is how they respond to large-scale modern cultivation of soybean. Description and monitoring of such soils is important in issues concerning understanding of the state and rate of change of carbon stock in this part of the terrestrial biosphere. ADEs have formed as a result of human action in the distant past and their key soil properties have been maintained for centuries. The introduction and expansion of large-scale mechanized agriculture in the Amazon have been regarded as fundamental problems from the antiquarian
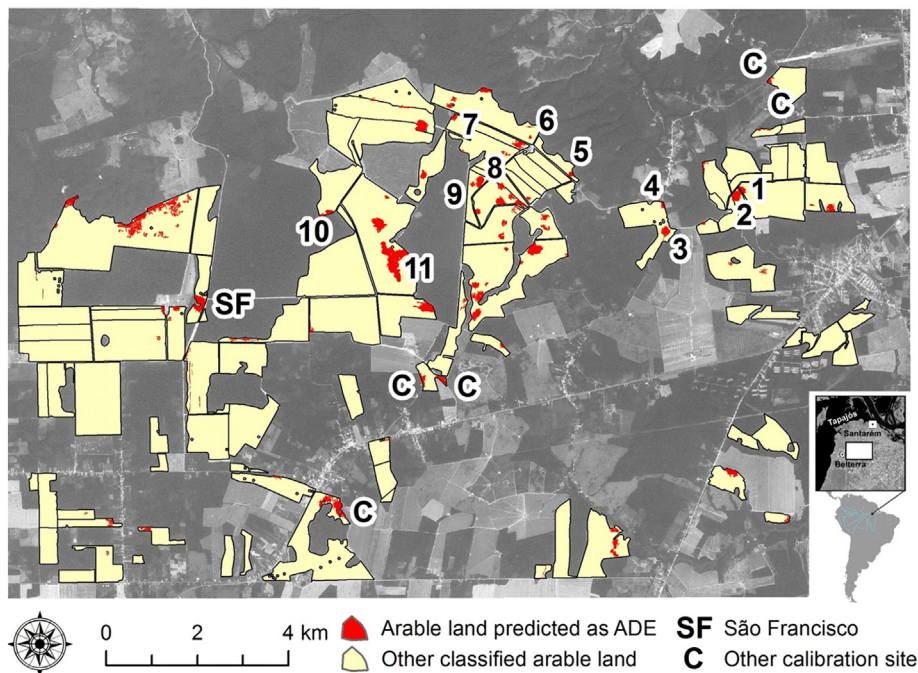

Fig. 6. Predicted locations with ADE on arable land with bare soil, November 27, 2012, in the study area on the Belterra Plateau. The numbers indicate ground-checked sites. The image in the background is the panchromatic band of the Spot 6 satellite image used in the classification modelling.

perspective to preserve this cultural heritage. Until very recently, archaeologists have only had a faint understanding of pre-Columbian archaeological sites in the Amazonian uplands (or *terra firme*) (e.g. through the limited but valuable work of Curt Nimuendajú on the Belterra Plateau in the 1920s [Nimuendajú, 2004]). The evidence now surfacing on the Belterra Plateau (Araújo et al., 2015; Mann, 2002; Schaan, 2016; Söderström et al., 2013; Stenborg et al., 2012) furthers our understanding of the pre-Columbian past, but it is ironic that the resource exploitation and infrastructural investments that are part of bringing this evidence to light are also the greatest threats to the preservation of the record. It is uncontroversial that tillage is destructive to non-buried archaeological sites; within the tilled layer archaeological strata, contexts and features are disturbed or obliterated, and artefacts and ecofacts are damaged and/or removed from their original position. As a result, the information potential of the archaeological record decreases. Deforestation in preparation of cropland and the mechanical work of agricultural machinery will impact negatively the preservation of affected ADE as a composite archaeological record. The value of exploited ADEs in terms of the archaeological information these provide is, however, a poorly investigated issue, in part since it is a recently realized problem. However, at São Francisco soil profile investigations indicated a shallow tilled layer depth of <20 cm, meaning that in more developed ADEs the lower archaeological strata remained essentially undisturbed from mechanical work; the archaeological strata extended well below the cultivation zone in the archaeological test excavation sites. Ceramics and other archaeological artefacts of the tilled zone are certainly not found in situ, but tests elsewhere indicate that artefact movement due to cultivation is mainly vertical, rather than horizontal (see e.g. Araujo, 2001; Isendahl and Olsson, 1996 and references cited therein). While disturbance is certainly significant, also disturbed and shallow ADEs maintain a (albeit lower) level of information potential on pre-Columbian activities. This and a range of other impacts need to be investigated in further detail. For instance, the application of fertilizers, e.g. phosphorous, may obscure the archaeological recording and interpretation of pre-Columbian element deposition. However, no significant such effect was visible in our studies of fields that have quite recently been brought under cultivation. Brought together, the impact of mechanized agriculture on ADE is fundamentally different from smallholder shifting cultivation practices to prepare the land, weed, plant and harvest manioc and other crops, even if these also involve a degree of topsoil disturbance. Developing robust methods to locate and map exploited ADEs by remote and proximal sensors is the first, necessary step in the process of evaluating how ADEs respond to mechanized agriculture.

5. Conclusions

Through a regional prediction model of ADE based on data from an optical, high-resolution satellite we located and delineated 17 previously unrecorded ADE sites larger than 2 ha in deforested land now used for agricultural production.

We showed that it was possible to calibrate data from both an EMI sensor and a handheld PXRF sensor to predict values of key ADE indicators. The most useful measurement variables were magnetic susceptibility (MSa) of the EMI sensor and Sr from the PXRF. If the sensor data were combined, it was possible to produce even better models for prediction of ADE properties.

Since the accessibility of the ADE sites is facilitated through the conversion to open cropland, paradoxically, the on-going land use-change that threatens the archaeological record may result in new opportunities for detailed studies.

Mapping currently exploited ADEs and monitoring changes in soil properties under different agricultural regimes, including different types of large-scale, mechanized agriculture, is of chief concern. The use of remote and proximal sensors improves the possibilities to do so.

References

Adamchuk, V.I., Allred, B., Doolittle, J., Grote, K., Viscarra Rossel, R.A., 2015. Tools for proximal soil sensing. In: Soil Survey Staff, Ditzler, C., West, L. (Eds.), Soil Survey Manual. Natural Resources Conservation Service. U.S. Department of Agriculture Handbook 18 (Available at www.nrcs.usda.gov/wps/portal/nrcs/detail/soils/scientists/?cid=nrcseprd329418. Accessed: 6 July 2015).

Araujo, A.G.M., 2001. Destruido pelo arado? Arqueologia de superficie e as armadilhas do senso comum. Rev. Arqueol. 14-15, 7–28.

Araújo, S.R., Söderström, M., Eriksson, J., Isendahl, C., Stenborg, P., Demattê, J.A.M., 2015. Determining soil properties in Amazonian Dark Earths by reflectance spectroscopy. Geoderma 237-238, 308–317.

Benech, C., Marmet, E., 1999. Optimum depth of investigation and conductivity response rejection of the different electromagnetic devices measuring apparent magnetic susceptibility. Archaeol. Prospect. 6, 31–45.

Blake, W.H., Wallbrink, P.J., Doerr, H., Shakesby, R.A., Humphreys, G.S., 2006. Magnetic enhancement in wildfire-affected soil and its potential for sediment-source ascription. Earth Surf. Process. Landf. 31, 249–264.

Boettinger, J.L., 2010. Environmental covariates for digital soil mapping in the western USA. In: Boettinger, J.L., Howell, D.W., Moore, A.C., Hartemink, A.E., Kienast-Brown, S. (Eds.), Digital Soil Mapping: Bridging Research, Environmental Application, and Operation. Springer, Berlin, pp. 17–27.

Bowen, H.J.M., Dymond, J.A., 1955. The uptake of calcium and strontium by plants from soils and nutrient solutions. J. Exp. Bot. 7, 264–272.

Clark, A., 1990. Seeing Beneath the Soil – Prospecting Methods in Archaeology. B.T. Batsford, London, UK.

Corrêa, J.A.J., Andrade, S.C.P., Pereira, I.C.N., 2011. Uso de imagens NDVI para análise temporal da dinâmica da paisagem no município de Belterra – PA. In: Neves Epiphanio, J.C., Soares Galvão, L. (Eds.), Anais XV Simpósio Brasileiro de Sensoriamento Remoto - SBSR, Curitiba, Brazil, 30 April - 5 May 2011. INPE, São José dos Campos, pp. 6540–6547.

Curi, N., Franzmeier, D.P., 1987. Effect of parent rocks on chemical and mineralogical properties of some Oxisols in Brazil. Soil Sci. Soc. Am. J. 51, 153–158.

Embrapa, 2009. Manual de análises químicas de solos, plantas e fertilizantes. Embrapa, Rio de Janeiro.

Eriksson, J., Söderström, M., Isendahl, C., 2016. Properties of Amazonian Dark Earths at Belterra Plateau, Pará, Brazil. In: Stenborg, P. (Ed.), Beyond Waters: Archaeology and Environmental History of the Amazonian Inland. GOTARC, Series A, Gothenburg Archaeological Studies vol. 6, pp. 87–98 Gothenburg.

Fearnside, P.M., Leal Filho, N., 2001. Soil and development in Amazonia: lessons from the biological dynamics of forest fragments project. In: Bierregaard, R.O., Gascon, C., Lovejoy, T.E., Mesquita, R.C.G. (Eds.), Lessons from Amazonia: The Ecology and Conservation of a Fragmented Forest. Yale University Press, New Haven, pp. 291–312.

Gee, G.W., Bauder, J.W., 1986. Particle size analysis. In: Klute, A. (Ed.), Methods of Soil Analysis: Part 1Physical and Mineralogical Methods. Soil Science Society of America, Madison, pp. 383–411.

Glaser, B., Birk, J.J., 2012. State of the scientific knowledge on properties and genesis of Anthropogenic Dark Earths in Central Amazonia (terra preta de Índio). Geochim. Cosmochim. Acta 82, 39–51.

Hastie, T., Tibshirani, R., Friedman, J., 2009. The Elements of Statistical Learning: Data Mining, Inference, and Prediction. second ed. Springer Series in Statistics, New York (746 p.).

Hornborg, A., 2009. Zero-sum world: challenges in conceptualizing environmental load displacement and ecologically unequal exchange in the world-system. Int. J. Comp. Sociol. 50, 237–262.

Irion, G., 1984. Clay minerals of Amazonian soils. In: Sioli, H. (Ed.), The Amazon: Limnology and Landscape Ecology of a Mighty Tropical River and Its BasinMonographie Biologicae Vol. 56. Dr W. Junk Publishers, Dordrecht, pp. 537–580.

Isendahl, C., Olsson, M., 1996. Matjordsarkeologi. In: Svensson, M., Karsten, P. (Eds.), Skåne, Malmöhus län, järnvägen Västkustbanan, delen Helsingborg–Kävlinge. Avsnittet Helsingborg–Landskrona (block 1–2). 1996. Arkeologisk förundersökning, UV Syd Rapport 1996:48. Central Board of National Antiquities, Lund, pp. 95–108.

IUSS Working Group WRB, 2014. World reference base for soil resources 2014. International Soil Classification System for Naming Soils and Creating Legends for Soil MapsWorld Soil Resources Reports No. 106. FAO, Rome.

Jordanova, N., Petrovsky, E., Kovacheva, M., Jordanova, D., 2001. Factors determining magnetic enhancement of burnt clay from archaeological sites. J. Archaeol. Sci. 28, 1137–1148.

Lehmann, J., 2007. A handful of carbon: commentary. Nature 447, 143–144.

Lehmann, J., Joseph, S., 2009. Biochar for Enviromental Management. Earthscan Publishing, Sterling, USA.

Mann, C.C., 2002. The real dirt on rainforest fertility. Science 297, 920–923.

Marwick, B., 2005. Element concentrations and magnetic susceptibility of anthrosols: indicators of prehistoric human occupation in the inland Pilbara, Western Australia. J. Archaeol. Sci. 32, 1357–1368.

McMichael, C.H., Palace, M.W., Bush, M.B., Braswell, B., Hagen, S., Neves, E.G., Silman, M.R., Tamanaha, E.K., Czarnecki, C., 2014. Predicting pre-Columbian anthropogenic soils in Amazonia. Proc. R. Soc. B 281, 20132475.

Milborrow, S., 2015. Notes on the Earth package. (Available at) www.milbo.org/doc/earth-notes.pdf (Accessed: July 6, 2015).

Minasny, B., McBratney, A.B., Lark, R.M., 2008. Digital soil mapping technologies for countries with sparse data infrastructure. In: Hartemink, A.E., McBratney, A.B., Mendonça-Santos, M.L. (Eds.), Digital Soil Mapping with Limited Data. Springer, Berlin, pp. 15–30.

Morton, D.C., DeFries, R.S., Shimabukuro, Y.E., Anderson, L.O., Arai, E., Bon Espirito-Santo, F., Freitas, R., Morisette, J., 2006. Cropland expansion changes deforestation dynamics in the southern Brazilian Amazon. Proc. Natl. Acad. Sci. U. S. A. 103, 14637–14641.

Nash, J.E., Sutcliffe, J.V., 1970. River flow forecasting through conceptual models part I: a discussion of principles. J. Hydrol. 10, 282–290.

Nimuendajú, C., 2004. In pursuit of a past Amazon: archaeological researches in the Brazilian Guyana and in the Amazon Region. In: Stenborg, P. (Ed.), Etnologiska Studier 45. Museum of World Culture, Gothenburg.

Potts, P.J., West, M., 2008. Portable X-Ray Fluorescence Spectrometry – Capabilities for In Situ Analysis. RSC Publishing, Cambridge, UK.

Quesada, C.A., Lloyd, J., Anderson, L.O., Fyllas, N.M., Schwarz, M., Czimczik, C.I., 2011. Soils of Amazonia with particular reference to the RAINFOR sites. Biogeosciences 8, 1415–1440.

R Core Team, 2014. R: A Language and Environment for Statistical Computing. R Foundation for Statistical Computing, Vienna, Austria http://www.R-project.org/. (Accessed 11 January 2015).

Richards, P., Pellegrina, H., VanWey, L., Spera, S., 2015. Soybean development: the impact of a decade of agricultural change on urban and economic growth in Mato Grosso, Brazil. PLoS One 10, 1–18.

Schaan, D.P., 2016. Discussing centre-periphery relations within the Tapajó domain, lower Amazon. In: Stenborg, P. (Ed.), Beyond Waters: Archaeology and Environmental History of the Amazonian Inland. GOTARC, Series A, Gothenburg Archaeological Studies vol. 6, pp. 23–36 Gothenburg.

Simpson, D., Van Meirvenne, M., Lück, E., Rühlmann, J., Saey, T., Bourgeois, J., 2010. Sensitivity of multi-coil frequency domain electromagnetic induction sensors to map soil magnetic susceptibility. Eur. J. Soil Sci. 61, 469–478.

Söderström, M., Eriksson, J., Isendahl, C., Araújo, S.R., Rebellato, L., Schaan, D.P., Stenborg, P., 2013. Using proximal soil sensors and fuzzy classification for mapping Amazonian Dark Earths. Agric. Food Sci. 22, 380–389.

Sombroek, W.G., 2000. Amazon land forms and soils in relation to biological diversity. Acta Amazon. 30, 81–100.

Steiner, C., Teixeira, W.G., Zech, W., 2004. Slash and char: an alternative to slash and burn practiced in the Amazon Basin. In: Glaser, B., Woods, W.I. (Eds.), Amazonian Dark Earths: Explorations in Space and Time. Springer, Berlin, pp. 183–194.

Stenborg, P., Schaan, D.P., Amaral Lima, M., 2012. Precolumbian land use and settlement pattern in the Santarém Region, Lower Amazon. Amazon. Rev. Antropol. 4, 222–250.

Stenborg, P., Schaan, D.P., Isendahl, C., Söderström, M., Eriksson, J., Amaral, M., Olvmo, M., 2014. The Cultivated Wilderness Project: hinterland archaeology in the Belterra Region, Pará, Brazil. In: Rostain, S. (Ed.), Antes de Orellana: Actas del 3er Encuentro Internacional de Arqueología Amazónica. Instituto Francés de Estudios Andinos, Lima, pp. 149–155.

Teixeira, W.G., Arruda, W., Lima, H.N., Iwata, S.A., Martins, G.C., 2008. Building a digital soil data base of the Solimões river region in the Brazilian Central Amazon. In: Hartemink, A.E., McBratney, A.B., Mendonça-Santos, M.L. (Eds.), Digital Soil Mapping with Limited Data. Springer, Berlin, pp. 327–335.

Thayn, J., Price, K.P., Woods, W.I., 2011. Locating Amazonian Dark Earths (ADE) using vegetation vigour as a surrogate for soil type. Int. J. Remote Sens. 32, 6713–6729.

Tite, M.S., Mullins, C., 1971. Enhancement of the magnetic susceptibility of soils on archaeological sites. Archaeometry 13, 209–219.

Verheijen, F., Jeffery, S., Bastos, A.C., Van der Velde, M., Diafas, I., 2010. Biochar Application to Soils: A Critical Scientific Review of Effects on Soil Properties, Processes and Functions. Institute for Environment and Sustainability, Ispra, Italy.

Weindorf, D.C., Zhu, Y., Chakraborty, S., Bakr, N., Huang, B., 2012a. Use of portable X-ray fluorescence spectrometry for environmental quality assessment of peri-urban agriculture. Environ. Monit. Assess. 184, 217–227.

Weindorf, D.C., Zhu, Y., McDaniel, P., Valerio, M., Lynn, L., Michaelson, G., Clark, M., Ping, C.L., 2012b. Characterizing soils via portable x-ray fluorescence spectrometer: 2. Spodic and albic horizons. Geoderma 189-190, 268–277.

WinklerPrins, A.M.G.A., Aldrich, S.P., 2010. Locating Amazonian Dark Earths: creating an interactive GIS of known locations. J. Lat. Am. Geogr. 9, 33–50.

Woods, W.I., Denevan, W.M., 2010. Amazonian Dark Earths: a first century report. In: Woods, W.I., Teixeira, W.G., Lehmann, J., Steiner, C., WinklerPrins, A.M.G.A., Rebellato, L. (Eds.), Amazonian Dark Earths: Wim Sombroek's Vision. Springer, Berlin, pp. 1–14.